Fast phase gates with trapped ions

M. Palmero,[1,*] S. Martínez-Garaot,[1] D. Leibfried,[2] D. J. Wineland,[2] and J. G. Muga[1]

[1]*Departamento de Química Física, UPV/EHU, Apartado Postal 644, 48080 Bilbao, Spain*
[2]*National Institute of Standards and Technology, 325 Broadway, Boulder, Colorado 80305, USA*

We implement faster-than-adiabatic two-qubit phase gates using smooth state-dependent forces. The forces are designed to leave no final motional excitation, independently of the initial motional state in the harmonic small-oscillations limit. They are simple, explicit functions of time and the desired logical phase of the gate, and are based on quadratic invariants of motion and Lewis-Riesenfeld phases of the normal modes.

I. INTRODUCTION

Realizing the full potential of quantum information processing requires a sustained effort to achieve scalability, and to make basic dynamical or logical operations faster, more accurate, and reliable under perturbations. Two-qubit gates are crucial building blocks in any scheme of universal quantum computing and have received much attention. An important step forward was the theoretical proposal of geometric gates with reduced sensitivity to the vibrational quantum numbers [1–4], with the first experimental realization in [5]. Soon after, Leibfried *et al.* [6] demonstrated a phase gate of the form

$$|\uparrow\uparrow\rangle \to |\uparrow\uparrow\rangle, \quad |\downarrow\downarrow\rangle \to |\downarrow\downarrow\rangle,$$
$$|\uparrow\downarrow\rangle \to i|\uparrow\downarrow\rangle, \quad |\downarrow\uparrow\rangle \to i|\downarrow\uparrow\rangle, \tag{1}$$

with two trapped ions of the same species subjected to state-dependent forces, where each spin-up or spin-down arrow represents an eigenstate of the σ_z operator for one of the ion qubits. Generalizations of this gate with the potential of reduced gate times were discussed by García-Ripoll *et al.* [7,8], and in [9–11]. The gate mechanism satisfies a number of desirable properties: it is insensitive to the initial motional state of the ions, at least in the small-oscillations regime where the motion is inside the Lamb-Dicke regime and the nonlinearities of the Coulomb coupling are negligible; it depends on "geometric" properties of the dynamics (phase-space areas), which makes it resistant to certain errors; it allows for close distances and thus strong interactions among the ions; and, finally, it may in principle be driven in short, faster-than-adiabatic times. The forces designed to make the ions return to their initial motional state in a rotating frame of phase-space coordinates [3,4] are different for different qubit state configurations, leading to qubit state dependent motional trajectories that produce a differential phase. Pulsed forces with abrupt kicks were designed [10,12–14], and also forces with discontinuous but finite derivatives [8,9,11], at boundary times of the entire operation, or between pulses, but in practice smooth continuous forces with continuous derivatives are desirable to minimize experimental errors.

In this paper, we revisit the phase gates and tackle the design of smooth forces as an inverse problem, via Lewis-Riesenfeld invariants [15]. For a predetermined operation time, the approach is applicable to arbitrary masses and proportionalities among the spin-dependent forces. This provides a more general scope than previous proposals to achieve faster than adiabatic operations. Hereafter, forces are assumed to be induced by off-resonant lasers that do not change the internal states. However, the basic ideas should be applicable to Mølmer and Sørensen type gates that flip the qubit spins during gates as well[1] [16]. Specifically we design forces to implement the operation

$$|\uparrow\uparrow\rangle \to e^{i\phi(\uparrow\uparrow)}|\uparrow\uparrow\rangle, \quad |\downarrow\downarrow\rangle \to e^{i\phi(\downarrow\downarrow)}|\downarrow\downarrow\rangle,$$
$$|\uparrow\downarrow\rangle \to e^{i\phi(\uparrow\downarrow)}|\uparrow\downarrow\rangle, \quad |\downarrow\uparrow\rangle \to e^{i\phi(\downarrow\uparrow)}|\downarrow\uparrow\rangle, \tag{2}$$

such that $\Delta\phi \equiv \phi(\uparrow\downarrow) + \phi(\downarrow\uparrow) - \phi(\uparrow\uparrow) - \phi(\downarrow\downarrow) = \pm\pi$, where the qubits could be realized with two different species, which may have practical importance to scale up quantum information processing with trapped ions [17]. Gates of the form (2) are computationally equivalent, up to single-qubit z rotations to the standard phase gate diag$[1,1,1,-1]$ written in the basis $\{|\uparrow\uparrow\rangle,|\uparrow\downarrow\rangle,|\downarrow\uparrow\rangle,|\downarrow\downarrow\rangle\}$ [18].

Our analysis demonstrates that invariant-based inverse Hamiltonian design is not limited to population control and may be adjusted for phase control as well. It was known that the phase of a given mode of the invariant (a time-dependent eigenstate of the invariant which is also a solution of the time-dependent Schrödinger equation) could be controlled [19], but the fact that "global phases," for a given internal state configuration, of arbitrary motional states can be controlled as well in a simple way had been overlooked. This is interesting for applying shortcuts to adiabaticity [20] in quantum information processing. In particular, we will derive ready-to-use, explicit expressions for the state-dependent forces, and may benefit from the design freedom offered by the invariant-based method to satisfy further optimization criteria.

To evaluate the actual performance of the phase gate at short times we have to compute fidelities, excitation energies, and/or their scaling behavior, according to the dynamics implied by the Hamiltonian including the anharmonicity of the Coulomb repulsion. This is important, as inversion protocols that work nearly perfectly in the small-oscillations regime fail for the large amplitudes of ion motion that occur in

---

*mikel.palmero@ehu.eus

---

[1]The Mølmer and Sørensen gate [1,4] can be mathematically described in the same language, replacing the eigenvectors of σ_z, $|\uparrow\rangle$, and $|\downarrow\rangle$, by the eigenvectors of σ_x, $|+\rangle$, and $|-\rangle$. This allows for an interchange of methods among the gate (2) and the Mølmer and Sørensen gate.

fast gates, and only a rough estimate of the domain of validity could be found in [8]. Here, we have numerically checked the validity of the phase gate up to gate times less than one oscillation period without assuming the approximations used in the small-amplitude regime. An additional perturbing effect with respect to an idealized limit of homogeneous spin-dependent forces is the position dependence of the forces induced by optical beams. This may be serious at the large motional amplitudes required for short gate times, when the ion motion amplitude becomes comparable to the optical wavelength as we illustrate with numerical examples.

The analytical theory for small oscillations is worked out in Secs. II, III, and IV. Then, we consider in Sec. V two ions of the same species, which implies some simplifications, assuming equal forces on both ions if they are in the same internal state, and opposite forces with equal magnitude when the ions are in different internal states (more general forces are treated in Appendix A). We also consider a more complete Hamiltonian including the anharmonicity of the Coulomb force and the spatial dependence of the light fields to find numerically the deviations with respect to ideal results within the small-oscillations approximation. Finally, in Sec. VI we study phase gates between ions of different species. The Appendices present generalizations of the results for arbitrary proportionalities between the state-dependent forces, alternative useful expressions for the phases, an analysis to determine the worst possible fidelities, the calculation of the width of the position of one ion in the two-ion ground state, and alternative inversion protocols.

II. THE MODEL

Consider two ions of charge e, masses m_1 and m_2, and coordinates x_1 and x_2, trapped within the same radially tight effectively one-dimensional trap. We assume the position x_1 of "ion 1" to fulfill $x_1 < x_2$ at all times due to Coulomb repulsion, with x_2 the position of "ion 2." Qubits may be encoded for each ion in two internal levels corresponding to the "spin-up" ($|\uparrow\rangle$) eigenstate of σ_z with eigenvalue $\sigma_i^z = 1$, and the "spin-down" eigenstate ($|\downarrow\rangle$) with eigenvalue $\sigma_i^z = -1$, $i = 1,2$. Off-resonant lasers induce state-dependent forces that are assumed first to be homogeneous over the extent of the motional state (Lamb-Dicke approximation). Later in the paper we shall analyze the effect of more realistic position-dependent light fields when the Lamb-Dicke condition is not satisfied. For a given spin configuration, $\uparrow\uparrow$, $\downarrow\downarrow$, $\uparrow\downarrow$, or $\downarrow\uparrow$, the Hamiltonian can be written as

$$\mathcal{H} = \frac{p_1^2}{2m_1} + \frac{1}{2}u_0 x_1^2 + F_1(t;\sigma_1^z)x_1$$
$$+ \frac{p_2^2}{2m_2} + \frac{1}{2}u_0 x_2^2 + F_2(t;\sigma_2^z)x_2$$
$$+ \frac{C_c}{x_2 - x_1} - E_0, \qquad (3)$$

where $C_c = \frac{e^2}{4\pi\epsilon_0}$, $u_0 = m_1\omega_1^2 = m_2\omega_2^2$, and ϵ_0 is the vacuum permittivity. A constant E_0 is added for convenience so that the minimum of

$$\mathcal{V} = \frac{1}{2}u_0 x_1^2 + \frac{1}{2}u_0 x_2^2 + \frac{C_c}{x_2 - x_1} - E_0 \qquad (4)$$

is at zero energy when x_1 and x_2 assume their equilibrium positions.

independent for different ions as they may be implemented by different lasers on different transitions. For equal-mass ions, the same lasers, and equal and opposite forces on the qubit eigenstates, they may simplify to $F_i = \sigma_i^z F(t)$. In principle, the proportionality between the force for the up and the down state could be different, but, as shown in Appendix A, the forces for a general proportionality can be related by a simple scaling to the ones found for the symmetric case $F_i = \sigma_i^z F(t)$.

We can determine normal modes for the zeroth-order Hamiltonian:

$$\mathcal{H}_0 = \frac{p_1^2}{2m_1} + \frac{p_2^2}{2m_2} + \mathcal{V}. \qquad (5)$$

The equilibrium positions of both ions under the potential $\mathcal{V}$ are

$$x_1^{(0)} = -\sqrt[3]{\frac{C_c}{4u_0}}, \quad x_2^{(0)} = \sqrt[3]{\frac{C_c}{4u_0}}, \qquad (6)$$

with equilibrium distance $x_0 = x_2^{(0)} - x_1^{(0)}$, which yields $E_0 = 3u_0 x_0^2/4$.

Diagonalizing the mass scaled curvature matrix $V_{ij} = \frac{1}{\sqrt{m_i m_j}} \frac{\partial^2 \mathcal{V}}{\partial x_i \partial x_j}\big|_{\{x_i,x_j\}=\{x_i^{(0)},x_j^{(0)}\}}$, that describes the restoring forces for small oscillations around the equilibrium positions, we get the eigenvalues

$$\lambda_\pm = \omega_1^2\left[1 + \frac{1}{\mu} \pm \sqrt{1 - \frac{1}{\mu} + \frac{1}{\mu^2}}\right], \qquad (7)$$

where $\omega_1 = (u_0/m_1)^{1/2}$ and $\mu = m_2/m_1$, with $\mu \geqslant 1$. The normal-mode angular frequencies are

$$\Omega_\pm = \sqrt{\lambda_\pm}, \qquad (8)$$

and the orthonormal eigenvectors take the form $v_\pm = \binom{a_\pm}{b_\pm}$, where

$$a_\pm = \left[\frac{1}{1 + \left(1 - \frac{1}{\mu} \mp \sqrt{1 - \frac{1}{\mu} + \frac{1}{\mu^2}}\right)^2 \mu}\right]^{1/2},$$

$$b_\pm = \left(1 - \frac{1}{\mu} \mp \sqrt{1 - \frac{1}{\mu} + \frac{1}{\mu^2}}\right)\sqrt{\mu}\, a_\pm \qquad (9)$$

fulfill

$$a_\pm^2 + b_\pm^2 = 1,$$
$$a_+ a_- + b_+ b_- = 0,$$
$$a_+ b_- - a_- b_+ = 1. \qquad (10)$$

The mass-weighted, normal-mode coordinates are

$$\mathsf{x}_+ = a_+\sqrt{m_1}\left(x_1 - x_1^{(0)}\right) + b_+\sqrt{\mu m_1}\left(x_2 - x_2^{(0)}\right),$$
$$\mathsf{x}_- = a_-\sqrt{m_1}\left(x_1 - x_1^{(0)}\right) + b_-\sqrt{\mu m_1}\left(x_2 - x_2^{(0)}\right), \qquad (11)$$

and the inverse transformation to the original position coordinates is

$$x_1 = \frac{1}{\sqrt{m_1}}(b_-\mathsf{x}_+ - b_+\mathsf{x}_-) - \frac{x_0}{2},$$

$$x_2 = \frac{1}{\sqrt{\mu m_1}}(-a_-\mathsf{x}_+ + a_+\mathsf{x}_-) + \frac{x_0}{2}. \qquad (12)$$

Finally, the Hamiltonian (3), neglecting higher-order anharmonic terms, and using conjugate "momenta" $\mathsf{p}_\pm = -i\hbar\partial/\partial\mathsf{x}_\pm$,[2] takes the form

$$\mathcal{H} = H_{NM} + \tilde{f}(t), \tag{13}$$

where

$$H_{NM} = H_+ + H_-,$$

$$H_\pm = \frac{\mathsf{p}_\pm^2}{2} + \frac{1}{2}\Omega_\pm^2\mathsf{x}_\pm^2 - f_\pm\mathsf{x}_\pm,$$

$$\tilde{f} = \frac{x_0}{2}(F_2 - F_1),$$

$$f_\pm(t) = \mp\frac{F_1 b_\mp}{\sqrt{m_1}} \pm \frac{F_2 a_\mp}{\sqrt{\mu m_1}}. \tag{14}$$

The function $\tilde{f}$ depends on time and on the internal states. By restricting the calculation to a given spin configuration, the dynamics may be worked out in terms of H_{NM} alone, $i\hbar\partial\psi_{NM}/\partial t = H_{NM}\psi_{NM}$, and the wave function that evolves with $\mathcal{H}$ in Eq. (13) is $e^{(-i/\hbar)\int_0^t dt' \tilde{f}}\psi_{NM}$. Purely time-dependent terms in the Hamiltonian are usually ignored as they imply global phases. In the phase-gate scenario, however, they are not really global, since they depend on the spin configuration. As the spin configuration may be changed after applying the phase gate, e.g., by resonant interactions, they may lead to observable interference effects and in general cannot be ignored. However, in the particular gate operation studied later the extra phase vanishes at the final time t_f, so we shall focus on the dynamics and phases generated by the Hamiltonian H_{NM}, which represents two independent forced harmonic oscillators with constant frequencies. We can now apply Lewis-Riesenfeld theory [15] in an inverse way [20]: The desired dynamics are designed first, and from the corresponding invariant the time-dependent functions in the Hamiltonian are inferred [21]. Note that in the inverse problem the oscillators are "coupled," as only one physical set of forces that will act on both normal modes of the uncoupled system must be designed [22].

III. ONE MODE

In this section we consider just one mode and drop the subscripts $\pm$ to make the treatment applicable to both modes. The goal is to find expressions for the corresponding invariants, dynamics, and phases. The Hamiltonian describing a harmonic oscillator with mass-weighted position and momentum is written as

$$H = H_0 + V, \tag{15}$$

$$H_0 = \frac{p^2}{2} + \frac{1}{2}\Omega^2 x^2, \tag{16}$$

$$V = -f(t)x. \tag{17}$$

Following the work of Lewis and Riesenfeld [15], it is possible to find a dynamical invariant of H solving the

equation

$$\frac{dI}{dt} \equiv \frac{\partial I}{\partial t} + \frac{1}{i\hbar}[I,H] = 0. \tag{18}$$

For a moving harmonic oscillator, a simple way to find an invariant is to assume a quadratic (in position and momentum) *Ansatz* with parameters that may be determined by inserting the *Ansatz* in Eq. (18). This leads to the invariant

$$I(t) = \frac{1}{2}(p - \dot{y})^2 + \frac{1}{2}\Omega^2(x - y)^2, \tag{19}$$

where the dot means "time derivative," and the function $y(t)$ must satisfy the differential (Newton) equation

$$\ddot{y} + \Omega^2 y = f, \tag{20}$$

so it can be interpreted as a "classical trajectory" (with dimensions $kg^{1/2}m$) in the forced harmonic potential [21].

This invariant is Hermitian, and has a complete set of eigenstates. Solving

$$I(t)\psi_n(t) = \lambda_n\psi_n(t), \tag{21}$$

we get the time-independent eigenvalues

$$\lambda_n = \hbar\Omega\left(\frac{1}{2} + n\right) \tag{22}$$

and the time-dependent eigenvectors

$$\psi_n(x,t) = e^{\frac{i}{\hbar}\dot{y}x}\phi_n(x - y), \tag{23}$$

where $\phi_n(x)$ is the nth eigenvector of the stationary oscillator,

$$\phi_n(x) = \frac{1}{\sqrt{2^n n!}}\left(\frac{\Omega}{\pi\hbar}\right)^{1/4} e^{\frac{-\Omega x^2}{2\hbar}} H_n\left(\sqrt{\frac{\Omega}{\hbar}}x\right), \tag{24}$$

and the H_n are Hermite polynomials. The Lewis-Riesenfeld phases θ_n must satisfy

$$\hbar\frac{d\theta_n}{dt} = \langle\psi_n|i\hbar\frac{\partial}{\partial t} - H|\psi_n\rangle, \tag{25}$$

so that the wave function (23) is indeed a solution of the time-dependent Schrödinger equation. Using Eq. (23), they are given by

$$\theta_n(t) = -\frac{1}{\hbar}\int_0^t dt'(\lambda_n + \dot{y}^2/2 - \Omega^2 y^2/2)$$
$$= -(n + 1/2)\Omega t - G(t), \tag{26}$$

where

$$G(t) = \frac{1}{2\hbar}\int_0^t dt'(\dot{y}^2 - \Omega^2 y^2). \tag{27}$$

Finally, the solution of the Schrödinger equation for the Hamiltonian H can be stated in terms of the eigenstate and Lewis-Riesenfeld phases of the invariant as

$$\psi(x,t) = \sum_n c_n e^{i\theta_n(t)}\psi_n(x,t). \tag{28}$$

Hereafter we consider that f is such that there are particular solutions $y = \alpha$ of Eq. (20) that satisfy at the boundary times $t_b = 0, t_f$ the boundary conditions

$$\alpha(t_b) = \dot{\alpha}(t_b) = 0. \tag{29}$$

---

[2]The dimensions of the mass-weighted coordinates are length times square root of mass, $mkg^{1/2}$, while the dimensions of the conjugate momenta are $kg^{1/2}m/s$.

They guarantee that all states $\Psi_n(x,t) = e^{i\theta_n(t)}\psi_n(x,t)$ end up at the original positions and at rest:

$$\Psi_n(x,t_f) = e^{i\theta_n(t_f)}\phi_n(x). \tag{30}$$

In other words, each initial eigenstate of the Hamiltonian is driven along a path that returns to the initial state with an added path-dependent phase. Moreover, we assume that the force vanishes at the boundary times $t_b = 0, t_f$, $f(t_b) = 0$, and, therefore, from Eq. (20),

$$\ddot{\alpha}(0) = \ddot{\alpha}(t_f) = 0. \tag{31}$$

Integrating by parts and using Eq. (20) as well as the boundary conditions $\alpha(t_b) = 0$, the phase factor common to all n takes the form

$$\phi(t_f) = -G(t_f) = \frac{1}{2\hbar}\int_0^{t_f} dt\, f\alpha. \tag{32}$$

To determine the stability of the results with respect to a systematic perturbation let us assume that the force is subjected to a homogeneous, small constant offset δ_f. Substituting $f \to f + \delta_f$, in first order, the phase shift is

$$\delta\phi(t_f) = \frac{\delta_f}{\hbar}\int_0^{t_f} dt\,\alpha. \tag{33}$$

Note that this could vanish if the zeroth-order trajectory α nullifies the integral, as it happens for the symmetrical functions used in this paper.

As the phases $\theta_n(t_f)$ in Eq. (26) have an extra n-dependent term, an arbitrary motional state $\psi(t)$ that superposes different n components does not generally return to the same initial projective ray. To remedy this it is useful to consider a rotating frame, i.e., we define $\psi_I(t) = e^{iH_0 t/\hbar}\psi(t)$, so that

$$\psi_I(t_f) = e^{-iG(t_f)}\psi_I(0), \tag{34}$$

with total phase $-G(t_f)$ for an arbitrary motional state. To decompose this phase into dynamical and geometric phases, we first note that

$$i\hbar\frac{\partial\psi_I}{\partial t} = V_I\psi_I, \tag{35}$$

where $V_I = -fe^{iH_0t/\hbar}xe^{-iH_0t/\hbar}$. The dynamical phase is

$$\begin{aligned}
\phi_d &= -\frac{1}{\hbar}\int_0^{t_f} dt\,\langle\psi_I(t)|V_I(t)|\psi_I(t)\rangle \\
&= -\frac{1}{\hbar}\int_0^{t_f} dt\,\langle\psi(t)|V(t)|\psi(t)\rangle \\
&= \frac{1}{\hbar}\int_0^{t_f} dt\, f(t)\langle x(t)\rangle. \tag{36}
\end{aligned}$$

The expectation value of x corresponds to a classical trajectory, i.e., to a solution of Eq. (20), but not necessarily the one corresponding to α. To describe a general trajectory it is useful to define dimensionless positions and momenta as

$$Y = \sqrt{\frac{\Omega}{2\hbar}}\,y, \quad P = \sqrt{\frac{1}{2\hbar\Omega}}\,p \tag{37}$$

(similarly for other coordinates such as x or α) as well as complex-plane combinations $z = Y + iP$.

The general solution of the position and momentum of a classical particle, or the corresponding expectation values for any quantum state, is compactly given in complex form as

$$\begin{aligned}
z_g(t) &= e^{-i\Omega t}\left\{z_g(0) + \frac{i}{\sqrt{2\hbar\Omega}}\int_0^t d\tau\, e^{i\Omega\tau} f\right\} \\
&= \tilde{z} + z_0, \tag{38}
\end{aligned}$$

where

$$\tilde{z} \equiv e^{-it\Omega}z_g(0), \tag{39}$$

$$z_0 \equiv \sqrt{\frac{\Omega}{2\hbar}}\,y_0 + i\sqrt{\frac{1}{2\Omega\hbar}}\,\dot{y}_0, \tag{40}$$

and y_0 is a particular solution satisfying $y_0(0) = \dot{y}_0(0) = 0$. For an f such that $y_0(t) = \alpha(t)$, and thus $z_0 = z_\alpha$, the boundary conditions at t_f are satisfied as well in the particular solution [see Eq. (29)]. By separating into real and imaginary parts, it can be seen that

$$\mathrm{Re}(\tilde{z})\frac{1}{\sqrt{2\Omega\hbar}}f = \frac{\partial\mathrm{Im}(z_\alpha\tilde{z}^*)}{\partial t}, \tag{41}$$

so that

$$\int_0^{t_f} dt\,\mathrm{Re}(\tilde{z})f = 0, \tag{42}$$

since $z_\alpha(t_b) = 0$. With these results, we rewrite Eq. (36) as

$$\phi_d = \frac{1}{\hbar}\int_0^{t_f} dt\left[\alpha + \sqrt{\frac{2\hbar}{\Omega}}\mathrm{Re}(\tilde{z})\right]f = \frac{1}{\hbar}\int_0^{t_f} dt\, f\alpha. \tag{43}$$

Therefore, the geometric phase ϕ_g is minus the total phase:

$$\phi_g = \phi - \phi_d = -\frac{1}{2\hbar}\int_0^{t_f} dt\, f\alpha = -\phi. \tag{44}$$

It is interesting to use the phase-space trajectory in the rotating frame $z_r = e^{i\Omega t}z_g = X_r + iP_r$ to write $f\langle x\rangle/\hbar = \sqrt{\frac{2}{\hbar\Omega}}\mathrm{Re}(z_g) = 2\mathrm{Im}(\frac{dz_r}{dt}z_r^*) = 4d\mathcal{A}/dt$, where $d\mathcal{A}$ is the differential of area swept in the rotating phase space, $d\mathcal{A}/dt = \frac{X_r}{2}\frac{dP_r}{dt} - \frac{P_r}{2}\frac{dX_r}{dt}$. Thus Eq. (36) becomes

$$\phi_d = 4\mathcal{A}. \tag{45}$$

Consequently, $\phi_g = -2\mathcal{A}$, and $\phi = 2\mathcal{A}$. The area is equal for all trajectories [values of $z_g(0)$] due to Eq. (42), so it may be calculated using $z_g(0) = 0$, i.e., the simple particular solution $z_g = z_\alpha$. Equations (44) and (45) are known results [8] but they are relevant for our work, so we have rederived them without using coherent states or a concatenation of displacement operators [6]. This is convenient when expressing the wave function as a superposition in an orthonormal basis.

IV. INVARIANT-BASED INVERSE HAMILTONIAN DESIGN

The results of the previous section may now be combined to inverse engineer the force. The Hamiltonian H_{NM} involves the two modes so that superscripts or subscripts have to be added to the functions of the previous section to denote the mode.

We assume that forces vanish at the boundary times $t_b = 0, t_f$, $F_1(t_b) = F_2(t_b) = 0$. Thus $f_\pm(t_b) = 0$. In the

rotating frame $\psi_I(t) = e^{iH_{NM}^0 t/\hbar}\psi_{NM}(t)$, where

$$H_{NM}^0 = H_+^0 + H_-^0, \quad H_\pm^0 = \frac{\mathsf{p}_\pm^2}{2} + \frac{1}{2}\Omega_\pm^2 \mathsf{x}_\pm^2, \quad (46)$$

so that

$$\psi_I(t_f) = e^{-i[G_-(t_f)+G_+(t_f)]}\psi_I(0). \quad (47)$$

Thus, the phase we are interested in for a given configuration is

$$\phi(t_f) = -[G_+(t_f) + G_-(t_f)]$$
$$= -\frac{1}{2\hbar}\int_0^{t_f} dt(\dot{\alpha}_+^2 + \dot{\alpha}_-^2 - \Omega_+^2\alpha_+^2 - \Omega_-^2\alpha_-^2)$$
$$= \frac{1}{2\hbar}\int_0^{t_f} dt(f_+\alpha_+ + f_-\alpha_-), \quad (48)$$

where the last step was done integrating by parts. An alternative double-integral expression used in Appendix A is shown in Appendix B. The inverse strategy is to design the $\alpha_\pm$ consistently with the boundary conditions, leaving free parameters that are fixed to produce the desired phase. The following section shows this in detail for equal masses.

V. EQUAL-MASS IONS

For two equal-mass ions, $m = m_1 = m_2$, $\omega = \omega_1 = \omega_2$, $a_+ = -b_+ = a_- = b_- = 1/\sqrt{2}$, $\Omega_- = \omega$ (center-of-mass mode), and $\Omega_+ = \sqrt{3}\omega$ (stretch mode). This implies [see Eq. (14)] that

$$f_\pm = \frac{\pm F_2 - F_1}{\sqrt{2m}}, \quad (49)$$

and F_1 and F_2 are defined as $F_i = \sigma_i^z F(t)$ (see the general case in Appendix A), so that the following values are found:

$$f_+(P) = f_-(A) = 0,$$
$$f_-(\uparrow\uparrow) = f_+(\uparrow\downarrow) = -2F/\sqrt{2m},$$
$$f_-(\downarrow\downarrow) = f_+(\downarrow\uparrow) = 2F/\sqrt{2m}, \quad (50)$$

where P stands for parallel spins, and A stands for antiparallel ones. If both ions have the same spin, then $f_+(P) = 0$ and no stretching is induced, but the center-of-mass ($-$) mode is transiently excited. In that case, $\alpha_+(P) = 0$ and

$$\alpha_-(\uparrow\uparrow) = -\alpha_-(\downarrow\downarrow), \quad (51)$$

according to Eqs. (20) and the established boundary conditions. For opposite spins $\alpha_-(A) = 0$, and only the stretching ($+$) mode is transiently excited. In that case

$$\alpha_+(\uparrow\downarrow) = -\alpha_+(\downarrow\uparrow). \quad (52)$$

The phase (48) takes two possible forms:

$$\phi(P) = \frac{1}{\hbar}\int_0^{t_f} dt \frac{-F}{\sqrt{2m}}\alpha_-(\uparrow\uparrow),$$
$$\phi(A) = \frac{1}{\hbar}\int_0^{t_f} dt \frac{-F}{\sqrt{2m}}\alpha_+(\uparrow\downarrow). \quad (53)$$

To inverse engineer the phase we use the *Ansatz* for $\alpha_+(\uparrow\downarrow;t)$ as a sum of Fourier cosines, with enough parameters to satisfy

all boundary conditions:

$$\alpha_+(\uparrow\downarrow;t) = a_0 + \sum_{n=1}^4 a_i \cos\left[\frac{(2n-1)\pi t}{t_f}\right]. \quad (54)$$

This is an odd function of $(t - t_f/2)$ which implies that $\ddot{\alpha}_+(\uparrow\downarrow;t)$, and thus $f_+(\uparrow\downarrow;t)$ are odd functions too with respect to the middle time of the process $t_f/2$. The parameters a_0, a_1, and a_2 are fixed to satisfy the corresponding boundary conditions for $\alpha_+(\uparrow\downarrow)$ in Eqs. (29) and (31):

$$a_0 = 0,$$
$$a_1 = 2a_3 + 5a_4,$$
$$a_2 = -3a_3 - 6a_4. \quad (55)$$

We get $f_+(\uparrow\downarrow;t)$ from Eq. (20), $f_+(\uparrow\downarrow;t) = \ddot{\alpha}_+(\uparrow\downarrow;t) + \Omega_+^2\alpha_+(\uparrow\downarrow;t)$. Due to the boundary conditions, $f_+(0) = f_+(t_f) = 0$. As $f_-(\uparrow\uparrow) = f_+(\uparrow\downarrow)$, we may solve Eq. (20) for $\alpha_-(\uparrow\uparrow;t)$ satisfying $\alpha_-(\uparrow\uparrow;t_b) = 0$, which, as can be seen in Eq. (20), will be different from $\alpha_+(\uparrow\downarrow;t)$ because the frequencies of both normal modes are different ($\Omega_+ \neq \Omega_-$), although the forces are equal [$\ddot{\alpha}_-(\uparrow\uparrow;t_b) = 0$ is automatically satisfied since $f_-(\uparrow\uparrow,t_b) = 0$]. The expression is rather lengthy but can be considerably simplified by imposing as well $\dot{\alpha}_-(\uparrow\uparrow;t_b) = 0$. This fixes a_3 as

$$a_3 = -\frac{5a_4(25\pi^2 - t_f^2\omega^2)}{49\pi^2 - t_f^2\omega^2}. \quad (56)$$

At this point $\alpha_+(\uparrow\downarrow;t)$ and $\alpha_-(\uparrow\uparrow;t)$ are left as functions of the parameter a_4:

$$\alpha_+(\uparrow\downarrow;t) = \frac{11\pi^2 + t_f^2\omega^2 + (49\pi^2 - t_f^2\omega^2)\cos\frac{2\pi t}{t_f}}{49\pi^2 - t_f^2\omega^2}$$
$$\times 32a_4 \cos\frac{\pi t}{t_f}\sin^4\frac{\pi t}{t_f},$$

$$\alpha_-(\uparrow\uparrow;t) = \frac{11\pi^2 + 3t_f^2\omega^2 + (49\pi^2 - 3t_f^2\omega^2)\cos\frac{2\pi t}{t_f}}{49\pi^2 - t_f^2\omega^2}$$
$$\times 32a_4 \cos\frac{\pi t}{t_f}\sin^4\frac{\pi t}{t_f}. \quad (57)$$

These are both odd functions with respect to $(t - t_f/2)$ and guarantee a vanishing final excitation in the two modes. They also have vanishing third derivatives at the time boundaries and thus imply the continuity in the force derivative at time boundaries, i.e., $\dot{F}(t_b) = 0$. Note that $-\frac{1}{\hbar}\int_0^{t_f} dt[\tilde{f}(A) - \tilde{f}(P)]$ vanishes [see Eq. (14)], since $\tilde{f}(P) = 0$ and $\tilde{f}(A)$ is also an odd function of $t - t_f/2$.

The differential phase takes the form [see Eq. (48)]

$$\Delta\phi \equiv 2[\phi(A) - \phi(P)]$$
$$= \frac{2}{\hbar}\int_0^{t_f} dt \frac{F}{\sqrt{2m}}[\alpha_-(\uparrow\uparrow) - \alpha_+(\uparrow\downarrow)]. \quad (58)$$

With the expressions (57) for $\alpha_+(\uparrow\downarrow)$ and $\alpha_-(\uparrow\uparrow)$ the integral can be solved to give

$$\Delta\phi = \frac{12a_4^2 t_f\omega^2(-2051\pi^4 + 476\pi^2 t_f^2\omega^2 - 33t_f^4\omega^4)}{\hbar(-49\pi^2 + t_f^2\omega^2)^2}. \quad (59)$$

Setting $\Delta\phi = \gamma$, the last free parameter is fixed as

$$a_4 = \pm\frac{1}{\omega}\left(-147\pi^2 + 3t_f^2\omega^2\right)\sqrt{\frac{\hbar}{6t_f}}$$

$$\times\left[\frac{\gamma/2}{-2051\pi^4 + 476\pi^2 t_f^2\omega^2 - 33t_f^4\omega^4}\right]^{1/2}. \quad (60)$$

The polynomial denominator in the last term is negative for all t_f (there are no real roots) so, to get a real a_4, γ must be chosen as a negative number. We choose $\gamma = -\pi$ to implement the gate (2). There are real solutions for a_4 for all t_f, no matter how small t_f is. In this sense there is no fundamental lower bound for the method, as long as the small amplitude and Lamb-Dicke approximations are valid. As for the sign alternatives in a_4, the different choices imply sign changes for the α and the forces. We, hereafter and in all figures, choose the positive sign. The resulting force takes the form

$$F(t) = \frac{g_1(t_f) + g_2(t_f)\cos\left(\frac{2\pi t}{t_f}\right) + g_3(t_f)\cos\left(\frac{4\pi t}{t_f}\right)}{t_f^2\sqrt{2051\pi^4 t_f\omega^2 - 476\pi^2 t_f^3\omega^4 + 33t_f^5\omega^6}}$$

$$\times 2\sqrt{2\pi\hbar m}\cos\left(\frac{\pi t}{t_f}\right)\sin^2\left(\frac{\pi t}{t_f}\right), \quad (61)$$

where

$$g_1(t_f) = 3\left(401\pi^4 - 36\pi^2 t_f^2\omega^2 + 3t_f^4\omega^4\right),$$
$$g_2(t_f) = -4\left(181\pi^4 - 76\pi^2 t_f^2\omega^2 + 3t_f^4\omega^4\right),$$
$$g_3(t_f) = 2401\pi^4 - 196\pi^2 t_f^2\omega^2 + 3t_f^4\omega^4, \quad (62)$$

which is shown in Fig. 1 for different values of t_f. [All simulations in this section are for two $^9\text{Be}^+$ ions and a trap frequency $\omega/(2\pi) = 2$ MHz.] The results are qualitatively similar to those found in [8] (also the asymptotic behavior for short operation times, $F \sim t_f^{-5/2}$) with a very different numerical method, but in our case the expression of F is explicit, has a continuous envelope, and the derivatives vanish at the edges, adding stability.

With this force, the trajectories of $\alpha_+(A)$ and $\alpha_-(P)$ [see Eqs. (51) and (52)] are given in Fig. 2 for two given times t_f in a dimensionless (quadrature) phase space, and in the rotating frame (the phase is twice the area swept in the rotating frame,
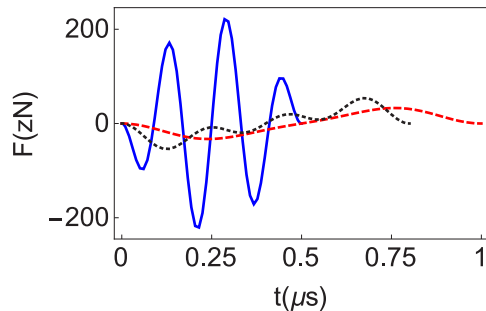

FIG. 1. $F(t)$ for two $^9\text{Be}^+$ ions in a trap with frequency $\omega/2\pi = 2$ MHz. $t_f = 0.5\,\mu$s (solid blue line), $t_f = 0.8\,\mu$s (dotted black line), and $t_f = 1\,\mu$s (dashed red line). The forces on each ion are state dependent, $F_i = \sigma_i^z F(t)$, $i = 1,2$.
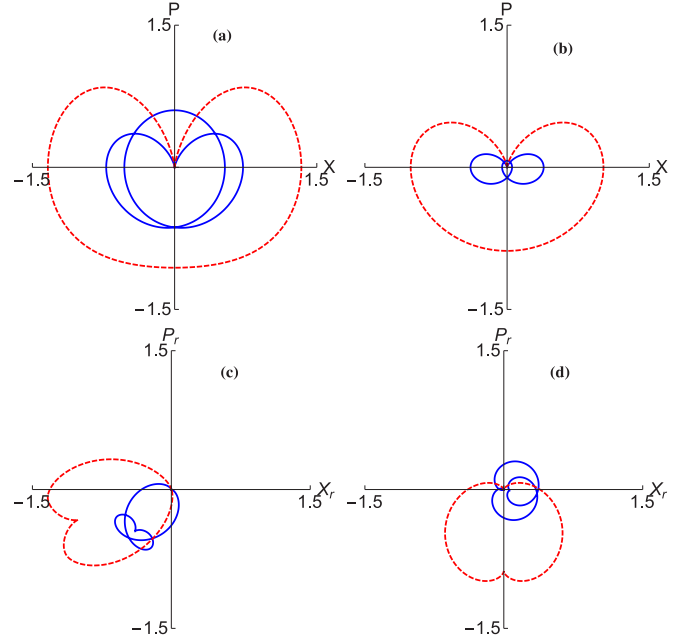

FIG. 2. Parametric plots of the quadratures, $X = \sqrt{\frac{\Omega_\pm}{2\hbar}}\alpha_\pm$ and $P = \sqrt{\frac{1}{2\hbar\Omega_\pm}}\dot{\alpha}_\pm$. The quadratures in the rotating frame are defined as $X_r = \text{Re}(e^{i\Omega_\pm t}Z)$, $P_r = \text{Im}(e^{i\Omega_\pm t}Z)$, where $Z = X + iP$. The solid blue lines represent the stretch $(+)$ mode for antiparallel spins and the dashed red lines represent the center-of-mass $(-)$ mode for parallel spins. (a) $t_f = 0.8\,\mu$s, (b) $t_f = 1\,\mu$s, (c) $t_f = 0.8\,\mu$s, and (d) $t_f = 1\,\mu$s in the rotating frame. The other parameters are chosen as in Fig. 1.

see Sec. III [8]). If the initial state is the ground state, they describe, respectively, the dynamics of the stretch mode for antiparallel spins and the center-of-mass mode for parallel spins. Notice that the trajectories lead to larger phase-space amplitudes for shorter times.

The phases within the harmonic (small amplitude) approximation are exact by construction for arbitrarily short times, but we should compare them with the phases when the system is driven by the full Hamiltonian (3) that contains the anharmonic Coulomb interaction. To that end we solve numerically the Schrödinger equation with the Hamiltonian (3) by using the "split-operator method" [23]. First, we fix the initial state as the ground state of the system $|\Psi_0\rangle$, which is found by making an initial guess and evolving it in imaginary time [24]. Then, the split-operator method is applied in real time to get the evolution of the wave function $|\Psi_t\rangle$. Phases are much more sensitive than populations to numerical errors, so we need a much shorter time step than the one usually required until the results converge. At the final time, the overlap $\mathcal{S} = \langle\Psi_0|\Psi_{t_f}\rangle$ between the initial and the final state, which depends on the spin configuration, is calculated. The phase of the overlap is defined as $\varphi_f = \arg\mathcal{S} \in [0,2\pi)$. In the quadratic approximation this includes a global term $-(\Omega_+ + \Omega_-)t_f/2$ [see Eq. (26)], absent in the rotating frame, that is canceled by calculating the phase differential between antiparallel and parallel spins, $2[\varphi_f(\uparrow\downarrow) - \varphi_f(\uparrow\uparrow)]$, displayed in Fig. 3. The corresponding infidelities, $1 - |\mathcal{S}|^2\cos^2(\Delta\phi - \pi) = 1 - \mathcal{F}$, are shown in Fig. 4 for the worst possible case, which
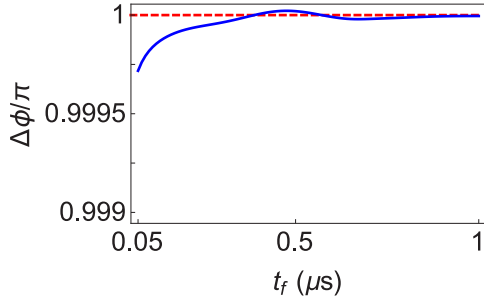
FIG. 3. $\Delta\phi$ for an exact evolution with the Hamiltonian in Eq. (3), and the target value of this phase (dashed red line). Same parameters as in Fig. 1. The initial motional state is the ground state.

is realized for an initial state with antiparallel spins (see Appendix C). The numerical results agree with the ideal result of the quadratic approximation reasonably well at least up to operation times ten times smaller than an oscillation period $2\pi/\omega$, i.e., 0.05 μs for the parameters considered. The approximation may hold for even shorter times, but they are very demanding computationally.

A different type of stability check is displayed in Fig. 5, where a realistic x-dependent sinusoidal force on each ion $F_i(t)\sin(\Delta k x + \pi/2)$ is considered instead of the homogeneous one. This force comes about because of the finite wavelength of the lasers used to generate the forces [6]. Close to the ground state, the motional wave function of the ion only overlaps with a small part of the optical wave which can then be approximated as having a constant gradient over the wave function (Lamb-Dicke approximation). In more excited motional states, this approximation breaks down and the sinusoidal shape of the light wave has to be taken into account. For driving a phase gate, the wave-vector difference Δk is adjusted so that the forces at the equilibrium positions $\pm x_0/2$ are the $F_i(t)$, with an integer number of periods $2\pi/\Delta k$ among them. Δk can be adjusted by changing the direction(s) of the beam(s) in laser-based experiments. We choose Δk so that the ions in the equilibrium position for the frequency $\omega/(2\pi) = 2$ MHz are placed in extrema of the sine function. In Figs. 5(a) and 5(b) we depict the differential phase and worst case fidelity versus t_f for this x-dependent force, starting in the motional ground state and performing the evolution for the full Hamiltonian as described in the previous paragraph. The two curves correspond to the ions being eight periods apart at equilibrium, similar to [6], or four periods apart. As
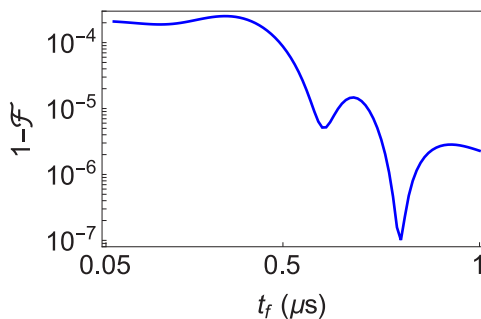

FIG. 4. Worst case infidelity vs final time, which is realized for the initial state $|\uparrow\downarrow\rangle$ [see Eq. (C8)]. Same parameters as in Fig. 1.
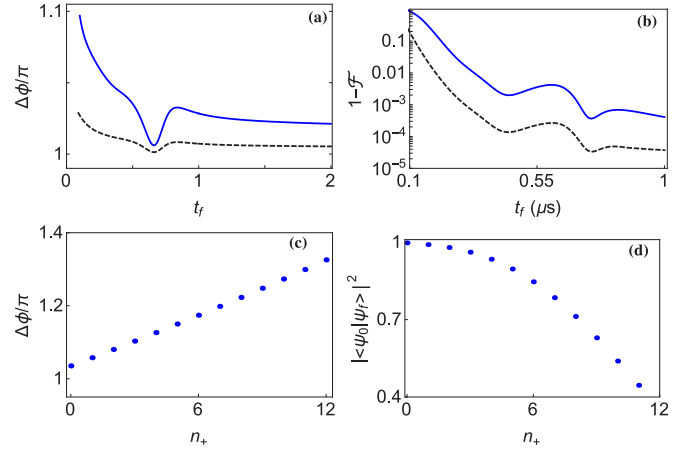

FIG. 5. Simulation of two ^{9}Be$^+$ ions with trap frequency $\omega/(2\pi) = 2$ MHz. Instead of homogeneous forces more realistic x-dependent forces $F_i(t)\sin(\Delta k x + \pi/2)$ are applied. In (a) and (b) the initial motional state is the ground state. $\Delta k = 8.67 \times 10^6$ m^{-1}, solid (blue) line (ions separated by eight lattice periods at equilibrium); $\Delta k = 4.33 \times 10^6$ m^{-1}, dashed (black) line (ions separated by four lattice periods). In (a) we display the final phase vs the final time. In (b) we display the worst case infidelity (realized for antiparallel spins). In (c) and (d) the phase and worst case fidelity (corresponding to antiparallel spins) for different initial excited states are depicted, for a time $t_f = 0.5$ μs and the ions separated by eight lattice periods.

expected, the results degrade for very short times faster than for the ideal homogeneous case represented in Fig. 4 since the ions explore a broader region where the forces deviate significantly from $F_i(t)$. The range of validity of the ideal results (the ones for a homogeneous force) in the limit $t_f\omega \ll 1$ is approximately given by $\frac{\Delta k}{\omega}\sqrt{\frac{\hbar}{t_f m}} \ll 1$, which may be found by estimating maximal amplitudes of $\alpha_\pm$ in Eq. (57), using Eq. (12) to calculate deviations from equilibrium positions, and comparing them to half a lattice period $\pi/\Delta k$. Note that for eight periods the phase does not really converge to the ideal value even at longer times, when the deviation is quite small compared to the period of the force. The reason is that the wave-function width also implies that the ions do not strictly experience a homogeneous force, which can lead to squeezing of the state of motion rather than just a coherent displacement. Starting with the ground-state wave function in the harmonic approximation (i.e., a product of ground-state wave functions for each mode), the width of the position of one ion is $\Delta x = \frac{1}{2}(1 + 1/\sqrt{3})^{1/2}\sqrt{\hbar/(m\omega)}$ (see Appendix D), which should be compared to $\pi/\Delta k$. For the parameters in Figs. 5(a) and 5(b) the ratios $\Delta x\,\Delta k/\pi$ are 0.04 (eight oscillations) and 0.02 (four oscillations).

In Figs. 5(c) and 5(d), the evolved state begins in some excited Fock state so that the Lamb-Dicke approximation breaks down more easily. We only consider excitations of the stretch mode, $|n_- = 0, n_+\rangle$, as the full Hamiltonian only has nonzero cubic terms for this mode.

We also study the scaling with t_f of spontaneous emission due to the transitions induced by intense off-resonant fields. The transition rate will be proportional to the intensity of the field, and to the effective potential acting on the ions, i.e., to $|F|$. In Fig. 6 we have integrated this quantity over time for
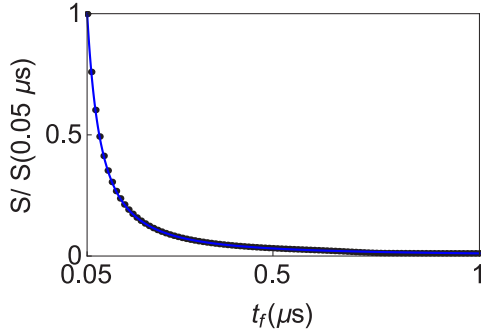
FIG. 6. $S = \int_0^{t_f} dt |F(t)|$ (dots). $F(t)$ is designed for equal-mass ions (^{9}Be$^+$ ions) according to Eq. (61) for a trap frequency $\omega/(2\pi) = 2$ MHz. The solid line is a fit proportional to $t_f^{-3/2}$.

different values of t_f. Since $F \sim t_f^{-5/2}$ the result scales as $t_f^{-3/2}$. We have normalized the integral by the force $|F(0.05\,\mu s)|$ as the scattering probability will depend on different factors which are not explicitly considered here such as Δk or the detuning.

Finally, in Table I we calculate the maximum value of the driving force in Eq. (61) for different ion species. Their potential performance for phase gates was analyzed in [9].

VI. DIFFERENT MASSES

For different mass ions, $m_1 = m$, $m_2 = \mu m$, and $u_0 = m\omega_1^2 = \mu m \omega_2^2$. In this case, due to their different structure, both ions will react to different laser fields, thus F_1 and F_2 can in principle be designed independently, such that $F_1 = \sigma_1^z F_a(t)$, $F_2 = \sigma_2^z F_b(t)$ (more general cases are studied in Appendix A), yielding

$$f_\pm(\uparrow\uparrow) = -f_\pm(\downarrow\downarrow) = \mp \frac{b_\mp}{\sqrt{m}} F_a \pm \frac{a_\mp}{\sqrt{\mu m}} F_b,$$

$$f_\pm(\uparrow\downarrow) = -f_\pm(\downarrow\uparrow) = \mp \frac{b_\mp}{\sqrt{m}} F_a \mp \frac{a_\mp}{\sqrt{\mu m}} F_b, \quad (63)$$

which, as in the previous section, implies that

$$\alpha_\pm(\downarrow\uparrow) = -\alpha_\pm(\uparrow\downarrow),$$
$$\alpha_\pm(\downarrow\downarrow) = -\alpha_\pm(\uparrow\uparrow) \quad (64)$$

TABLE I. Maximum value of the force F in Eq. (61) for different ions, and their corresponding mass and trap frequency. The parameters were chosen so that they all have the same spring constant. The calculated maximum force is for an operation time $t_f = 0.5\,\mu s$.

	m (a.u.)	$\omega/(2\pi)$ (MHz)	$F_{\max}$ (zN)
Be	9	2	223.89
Mg	24	$2\sqrt{\frac{9}{24}}$	656.85
Ca	40	$2\sqrt{\frac{9}{40}}$	1119.89
Sr	88	$2\sqrt{\frac{9}{88}}$	2511.53
Ba	138	$2\sqrt{\frac{9}{138}}$	3961.61
Yb	172	$2\sqrt{\frac{9}{172}}$	4947.72

[see Eqs. (14) and (20)], so if the protocol is designed to satisfy the boundary conditions for the $\uparrow\downarrow$ and $\uparrow\uparrow$ configurations, it will automatically satisfy the conditions for the remaining configurations. Inversely, from Eqs. (63) and (10),

$$F_a = -\sqrt{m}[a_- f_-(\uparrow\downarrow) + a_+ f_+(\uparrow\downarrow)],$$
$$F_b = \sqrt{\mu m}[b_- f_-(\uparrow\downarrow) + b_+ f_+(\uparrow\downarrow)]. \quad (65)$$

The procedure to design the forces is summarized in the following scheme:

$$\alpha_\pm(\uparrow\downarrow) \dashrightarrow f_\pm(\uparrow\downarrow) \dashrightarrow F_a, F_b \dashrightarrow f_\pm(\uparrow\uparrow) \dashrightarrow \alpha_\pm(\uparrow\uparrow). \quad (66)$$

To start with, *Ansätze* are proposed for $\alpha_+(\uparrow\downarrow)$ and $\alpha_-(\uparrow\downarrow)$:

$$\alpha_+(\uparrow\downarrow) = a_0 + \sum_{n=1}^{4} a_n \cos\left[\frac{(2n-1)\pi t}{t_f}\right],$$
$$\alpha_-(\uparrow\downarrow) = 0. \quad (67)$$

It is also possible to design them so as to cancel $\alpha_+(\uparrow\downarrow) = 0$ instead of $\alpha_-(\uparrow\downarrow)$, as discussed in Appendix E. Similarly to the previous section, a_0, a_1, and a_2 are fixed to satisfy the boundary conditions for $\alpha_+(\uparrow\downarrow)$ in Eqs. (29) and (31):

$$a_0 = 0, \quad a_1 = 2a_3 + 5a_4, \quad a_2 = -3a_3 - 6a_4. \quad (68)$$

Introducing these *Ansätze* in Eq. (20), expressions for $f_\pm(\uparrow\downarrow; t)$ are found, in particular $f_-(\uparrow\downarrow) = 0$, and from these, expressions for the control functions $F_a(t), F_b(t)$ follow according to Eq. (65). Since $\alpha_+(t)(\uparrow\downarrow)$ is an odd function of $(t - t_f/2)$, the same symmetry applies to $F_a(t)$, $F_b(t)$, and to the spin-dependent forces F_1, F_2. Thus the time integral of $\tilde{f}$ [see Eq. (14)] is zero for different masses as well and does not contribute to the phase.

Using the last line of Eq. (14), the effective forces $f_\pm(\uparrow\uparrow)$ are found. Plugging these functions into Eq. (20) we solve the differential equations imposing the boundary conditions $\alpha_\pm(\uparrow\uparrow; t_b) = 0$ to fix the integration constants. At this point the boundary conditions for $\ddot{\alpha}_\pm(\uparrow\uparrow; t_b)$ are automatically satisfied, and $\dot{\alpha}_\pm(\uparrow\uparrow; 0) = \dot{\alpha}_\pm(\uparrow\uparrow; t_f)$ by symmetry. Thus, imposing that the first derivatives vanish at the boundary times, a_3 is fixed as

$$a_3 = \frac{-25\pi^2 + t_f^2 \Omega_-^2}{49\pi^2 - t_f^2 \Omega_-^2} 5a_4. \quad (69)$$

Once the $\alpha_\pm$ are given for both configurations, such that they do not produce any excitation in the modes at the final time, the final phase difference is, as in the previous section,

$$\Delta\phi(t_f) = 2[\phi(A) - \phi(P)]$$
$$= -\frac{1}{\hbar} \sum_{\mu=\pm} \int_0^{t_f} dt \left[\dot{\alpha}_\mu^2(\uparrow\downarrow) - \Omega_\mu^2 \alpha_\mu^2(\uparrow\downarrow)\right]$$
$$+ \frac{1}{\hbar} \sum_{\mu=\pm} \int_0^{t_f} dt \left[\dot{\alpha}_\pm^2(\uparrow\uparrow) - \Omega_\mu^2 \alpha_\mu^2(\uparrow\uparrow)\right]. \quad (70)$$

The integrals can be evaluated and give a function of a_4. This parameter is finally set by imposing some value to the phase

difference, $\Delta\phi(t_f) = \gamma$:

$$a_4 = \sqrt{\frac{\gamma\hbar(1 + (-1+\mu)\mu)\left(-49\pi^2 + t_f^2\Omega_-^2\right)^2}{\Delta}},$$

$$\Delta = 6\mu(\Omega_- - \Omega_+)(\Omega_- + \Omega_+)t_f\left[2051\pi^4 \right.$$
$$\left. + 11t_f^4\Omega_-^2\Omega_+^2 - 119\pi^2 t_f^2(\Omega_-^2 + \Omega_+^2)\right]. \quad (71)$$

The function Δ has zeros at

$$t_f^{(0)} = 0,$$

$$t_f^{(1)} = \pm\pi\sqrt{\frac{119(\Omega_-^2 + \Omega_+^2) - \delta}{22\Omega_-^2\Omega_+^2}},$$

$$t_f^{(2)} = \pm\pi\sqrt{\frac{119(\Omega_-^2 + \Omega_+^2) + \delta}{22\Omega_-^2\Omega_+^2}}, \quad (72)$$

where

$$\delta = \sqrt{7(2023\Omega_-^4 - 8846\Omega_-^2\Omega_+^2 + 2023\Omega_+^4)}. \quad (73)$$

Considering only the positive times, in the intervals $(t_f^{(0)}, t_f^{(1)})$ and $t_f > t_f^{(2)}$, Δ is negative, so we chose $\gamma = -\pi$ to make a_4, and thus F_a, F_b, real. In the interval $(t_f^{(1)}, t_f^{(2)})$ Δ is positive, so we can choose $\gamma = \pi$.

The explicit expressions for the control functions are finally, from Eq. (65),

$$F_a = \left[g_1^a + g_2^a \cos\left(\frac{2\pi t}{t_f}\right) + g_3^a \cos\left(\frac{4\pi t}{t_f}\right)\right]$$
$$\times \frac{8a_4 a_+ \sqrt{m}\cos\left(\frac{\pi t}{t_f}\right)\sin^2\left(\frac{\pi t}{t_f}\right)}{-49\pi^2 t_f^2 + t_f^4\Omega_-^2},$$

$$F_b = -\frac{b_+\sqrt{\mu}}{a_+}F_a, \quad (74)$$

where

$$g_1^a = 3\left[401\pi^4 + t_f^4\Omega_-^2\Omega_+^2 - 9\pi^2 t_f^2(\Omega_-^2 + \Omega_+^2)\right],$$

$$g_2^a = 4\left[-181\pi^4 - t_f^4\Omega_-^2\Omega_+^2 + 19\pi^2 t_f^2(\Omega_-^2 + \Omega_+^2)\right], \quad (75)$$

$$g_3^a = \left(49\pi^2 - t_f^2\Omega_-^2\right)\left(49\pi^2 - t_f^2\Omega_+^2\right).$$

F_a, F_b diverge for the final times in Eq. (72), so these times must be avoided. The positions of the divergences depend on the chosen *Ansatz*. In particular, for a polynomial, rather than cosine *Ansatz*, the only divergence is at $t_f = 0$. We have, however, kept the cosine *Ansatz* as it needs fewer terms and it simplifies the results and the treatment of boundary conditions.

Figure 7 shows the phase found numerically with the exact Hamiltonian for ^{9}Be (ion 1) and ^{25}Mg (ion 2) in the Lamb-Dicke limit beginning in the ground motional state. Figure 8 shows the quadratures for such a protocol at final time $t_f = 0.5\,\mu$s, and Fig. 9 shows the worst case infidelities at final time, which, as in the previous section, correspond to initial states with antiparallel spin (see Appendix C). Around an oscillation period $2\pi/\omega_1 = 0.5\,\mu$s, the results are slightly worse than in the previous section for equal-mass ions, but still with a high
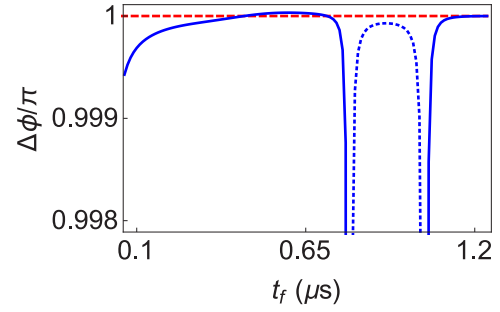

FIG. 7. Total final phase $\Delta\phi$ in Eq. (70) vs the final time (solid and dotted blue lines) for an exact wave function evolving with the Hamiltonian in Eq. (3), and the target value of this phase (dashed red line). The simulation is done for a ^{9}Be$^+$ and a ^{25}Mg$^+$ ion, initially in the motional ground state, within a trap of frequency $\omega_1/(2\pi) = 2$ MHz. At final times $t_f \sim 0.8$ and $1.03\,\mu$s we change solutions [see the discussion below Eq. (73)]. The solid line is for $\gamma = -\pi$ and the dashed line is for $\gamma = \pi$.

fidelity. For final times close to $t_f^{(1)} \sim 0.8\,\mu$s and $t_f^{(2)} \sim 1.03\,\mu$s the solutions change, with a drop in the stability of the phase (Fig. 7) and in the fidelity (Fig. 9). The phase and fidelity improve and stabilize again for times $t_f > 1.03\,\mu$s.

In the limit where both ions are equal, $F_a = F_b = F$, and the results of the previous section are found consistently.

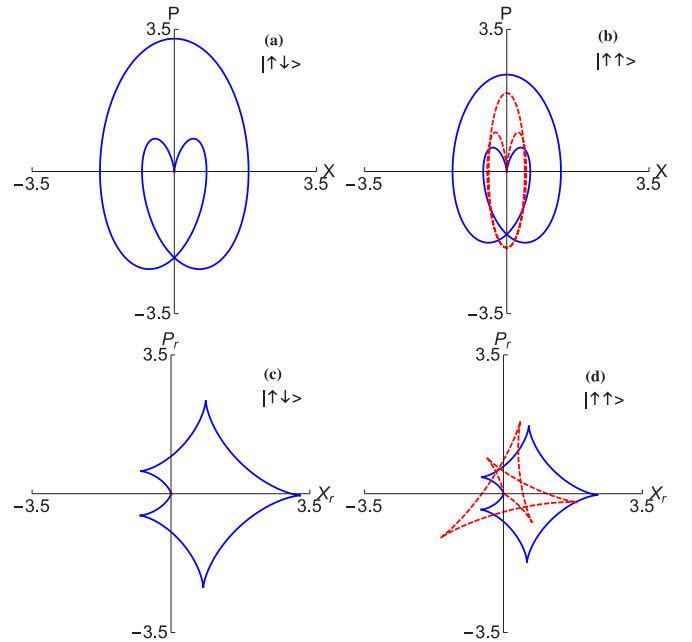
FIG. 8. Parametric plots of the quadratures, $X = \sqrt{\frac{\Omega_\pm}{2\hbar}}\alpha_\pm$ and $P = \sqrt{\frac{1}{2\hbar\Omega_\pm}}\dot{\alpha}_\pm$. The quadratures in the rotating frame are defined as $X_r = \text{Re}(e^{i\Omega_\pm t}Z)$, $P_r = \text{Im}(e^{i\Omega_\pm t}Z)$, where $Z = X + iP$ at $t_f = 0.5\,\mu$s. The solid blue lines represent the stretch (+) mode and the dashed red lines represent the center-of-mass (−) mode. (a) and (c) represent the phase-space trajectory for $|\uparrow\downarrow\rangle$ and $|\downarrow\uparrow\rangle$, in the normal and the rotating frame, respectively, while (b) and (d) represent the phase-space trajectories for $|\uparrow\uparrow\rangle$, in the normal and rotating frames, respectively. The other parameters are chosen as in Fig. 7.
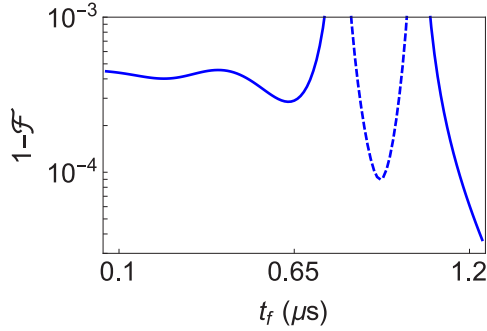
FIG. 9. Infidelity vs final time for the worst case, which corresponds to antiparallel spins [see Eq. (C8)]. Same parameters as in Fig. 7. The solid line is for $\gamma = -\pi$ and the dashed line is for $\gamma = \pi$.

VII. DISCUSSION

In this paper, we have designed simple and explicit protocols to perform fast and high fidelity phase gates with two trapped ions by using the invariant-based method to bypass adiabaticity. The scheme of the gate expands on methods that have been already tested in the laboratory. Experimentally, the state-dependent forces may be created by a standing wave with time-varying intensity produced by two crossed laser beams the amplitude of which is modulated following a smoothly designed trajectory to excite motion in both normal modes. In the limit of small oscillations, we can use both a normal-mode harmonic approximation and the Lamb-Dicke limit and apply the inverse-design method assuming homogeneous forces. We have also numerically simulated the system dynamics and gate behavior without these approximations, namely, including the anharmonicity and the position dependence of the forces. Good fidelities are obtained at times around 1 μs, which is a significantly shorter time compared to the best experimental results so far and close to the center-of-mass oscillation period which was assumed to be 0.5 μs in this work. Moreover, state-of-the-art technology allows for higher trap frequencies than those used in our simulations, which should further improve the results. Expressions for the forces have been found for different scenarios, specifically for equal or different masses, as well as for different proportionality factors between the spin-dependent forces.

At present, technical limitations for the laser intensity and Raman detuning will constrain the shortest gate times that can be reached. However, technical limitations can change, especially if there is motivation to push them. The goal of our paper is to also explore the possibilities that exist beyond what is presently doable.

Extensions of this work are possible in several directions. For example, the deviations from the ideal conditions may be taken into account to design the forces. The force design given here, based on symmetrical trajectories of the modes, gives already stable results (a vanishing first-order correction to the phase) with respect to a systematic, homogeneous deviation of the forces [see Eq. (33)]. Moreover the freedom offered by the approach may also be used to choose stable protocols with respect to different noises and perturbations (see, e.g., [25–28]).

APPENDIX A: GENERALIZATION FOR AN ARBITRARY FORCE RATIO

1. Equal-mass ions

In the main text we have studied state-dependent forces which are equal and opposite to each other for up and down spins, $F_i = \sigma_i^z F(t)$. However, depending on laser beam polarization and specific atomic structure, different proportionalities among the two forces will arise. Let us consider a general force ratio $F_i(\uparrow) = -c\tilde{F}(t)$ and $F_i(\downarrow) = -\tilde{F}(t)$, where c is a constant. Then, for equal-mass ions, instead of Eq. (50) (corresponding to $c = -1$), we find [see Eq. (49)]

$$f_+(\uparrow\uparrow) = f_+(\downarrow\downarrow) = 0,$$

$$f_-(\uparrow\uparrow) = cf_-(\downarrow\downarrow) = \frac{2\tilde{F}c}{\sqrt{2m}},$$

$$f_+(\uparrow\downarrow) = -f_+(\downarrow\uparrow) = -\frac{1-c}{\sqrt{2m}}\tilde{F},$$

$$f_-(\uparrow\downarrow) = f_-(\downarrow\uparrow) = \frac{1+c}{\sqrt{2m}}\tilde{F}. \tag{A1}$$

To inverse engineer the forces we start choosing the same *Ansatz* for $\alpha_+(\downarrow\uparrow)$ as in Eq. (54). a_0 through a_2 are also fixed in the same manner to satisfy the boundary conditions. Using Eq. (20) this gives $f_+(\downarrow\uparrow; t)$ as a function of a_3, a_4, and in fact all other $f_\pm$ by scaling them according to Eq. (A1). As in the main text, the same a_3 in Eq. (56) guarantees that $\dot{\alpha}_\pm(t_b) = 0$ for all spin configurations. Now, using Eq. (48) we can write down the phase produced by each spin configuration. Individually, they depend on c but, adding them all in $\Delta\phi = \phi(\uparrow\downarrow) + \phi(\downarrow\uparrow) - \phi(\uparrow\uparrow) - \phi(\downarrow\downarrow)$, the dependence on c is canceled, as can be seen from Eq. (B1) or Eqs. (20) and (A1). Following the method described in the main text, imposing $\Delta\phi = \gamma$ fixes the remaining parameter a_4, so that the same expression in Eq. (60) is found. Using Eqs. (50) and (A1), the generic control function $\tilde{F}$ is simply proportional to that for $c = -1$ [see Eq. (61)]:

$$\tilde{F} = \frac{2}{1-c}F. \tag{A2}$$

2. Different masses

Similarly, for different-mass ions in the generic case both ions could have different proportionality factors for the spin-dependent forces:

$$F_1(\uparrow) = -c_1\tilde{F}_a, \quad F_1(\downarrow) = -\tilde{F}_a,$$

$$F_2(\uparrow) = -c_2\tilde{F}_b, \quad F_2(\downarrow) = -\tilde{F}_b. \tag{A3}$$

Instead of Eq. (63), the normal-mode forces are now [see Eq. (14)]

$$f_\pm(\uparrow\uparrow) = \pm\frac{b_\mp}{\sqrt{m}}c_1\tilde{F}_a \mp \frac{a_\mp}{\sqrt{\mu m}}c_2\tilde{F}_b,$$

$$f_\pm(\uparrow\downarrow) = \pm\frac{b_\mp}{\sqrt{m}}c_1\tilde{F}_a \mp \frac{a_\mp}{\sqrt{\mu m}}\tilde{F}_b,$$

$$f_\pm(\downarrow\uparrow) = \pm\frac{b_\mp}{\sqrt{m}}\tilde{F}_a \mp \frac{a_\mp}{\sqrt{\mu m}}c_2\tilde{F}_b,$$

$$f_\pm(\downarrow\downarrow) = \pm\frac{b_\mp}{\sqrt{m}}\tilde{F}_a \mp \frac{a_\mp}{\sqrt{\mu m}}\tilde{F}_b. \tag{A4}$$

This implies that the $\alpha_\pm$ are in general all different and the inverse scheme in Eq. (66) is replaced by

$$\alpha_\pm(\uparrow\downarrow) \dashrightarrow f_\pm(\uparrow\downarrow)$$

$$\dashrightarrow \tilde{F}_a, \tilde{F}_b \dashrightarrow \begin{cases} f_\pm(\uparrow\uparrow) \dashrightarrow \alpha_\pm(\uparrow\uparrow) \\ f_\pm(\downarrow\uparrow) \dashrightarrow \alpha_\pm(\downarrow\uparrow). \\ f_\pm(\downarrow\downarrow) \dashrightarrow \alpha_\pm(\downarrow\downarrow) \end{cases} \tag{A5}$$

$$\underbrace{\qquad\qquad\qquad\qquad\qquad\qquad}_{\text{functions of } c_1, c_2}$$

Using Eqs. (10) and (A4) we may rewrite the control functions $\tilde{F}_a$ and $\tilde{F}_b$ as

$$\tilde{F}_a = \sqrt{m}[a_- f_-(\uparrow\downarrow) + a_+ f_+(\uparrow\downarrow)]/c_1,$$

$$\tilde{F}_b = \sqrt{\mu m}[b_- f_-(\uparrow\downarrow) + b_+ f_+(\uparrow\downarrow)]. \tag{A6}$$

As in the special case $c_1 = c_2 = -1$ of the main text, we use the *Ansätze* in Eq. (67) for $\alpha_\pm(\uparrow\downarrow)$, and the parameters in Eq. (68). In particular $\alpha_-(\uparrow\downarrow) = 0$ and $f_-(\uparrow\downarrow) = 0$, so $\tilde{F}_a$ and $\tilde{F}_b$ are proportional to each other [see Eq. (A6)], and thus all the $f_\pm$ are proportional to $f_+(\uparrow\downarrow)$ according to Eq. (A4). Thus, from Newton's equations, all (nonzero) solutions $\alpha_+(t)$ are proportional to each other, and similarly all (nonzero) $\alpha_-(t)$ are proportional to each other. The parameter choice in Eq. (68) assures that $\alpha_+(t_b) = \dot{\alpha}_+(t_b) = 0$ for all configurations. Fixing, for example, $\alpha_-(\uparrow\uparrow)(t_b) = 0$, a_3 may be fixed as in Eq. (69), so that $\dot{\alpha}_-(t_b) = 0$, and therefore $\alpha_-(t_b) = \dot{\alpha}_-(t_b) = 0$ as well for all configurations. Using Eq. (48) to calculate the phases, and imposing $\Delta\phi = \gamma$, the remaining parameter (a_4) is fixed as

$$a_4 = C a_4^0, \tag{A7}$$

where $a_4^0 \equiv a_4(c_1 = c_2 = -1)$ is given in Eq. (71) and

$$C = 2\sqrt{\frac{-c_1}{(c_1 - 1)(c_2 - 1)}}. \tag{A8}$$

All coefficients in $\alpha_+(\uparrow\downarrow)$ are proportional to a_4, so $\alpha_+(\uparrow\downarrow)$ is just scaled by the factor C with respect to the ones for $c_1 = c_2 = -1$ in the main text, and $f_+(\uparrow\downarrow)$ is also scaled by the same factor according to Eq. (20). Comparing Eqs. (A6) and (65), and using $f_-(\uparrow\downarrow) = 0$, we find that

$$\tilde{F}_a = -\frac{C}{c_1}F_a,$$

$$\tilde{F}_b = C F_b. \tag{A9}$$

in terms of the forces F_a, F_b given in Eq. (74) for $c_1 = c_2 = -1$. All these functions have odd symmetry with respect to the middle time $t_f/2$ so that there is no contribution to the phase from the time integral of $\tilde{f}$ [see Eq. (14)].

Finally, let us analyze the limit of equal masses where $c_1 = c_2 = c$ and $\mu = 1$. In the main text, this implies $c_1 = c_2 = c = -1$ and $F_a(\mu \to 1) = F_b(\mu \to 1) = F$, in agreement with the physical constraint of using the same laser for both ions. However, when $c \neq 1$, $\tilde{F}_a(\mu \to 1) \neq \tilde{F}_b(\mu \to 1)$ [see Eq. (A9)]. Physically this implies the use of two different lasers which is not possible in practice, so equal masses with $c \neq 1$ have to be treated separately, as specified in Sec. A1.

APPENDIX B: INTEGRAL EXPRESSION FOR THE PHASE

For $\alpha_\pm(0) = \dot{\alpha}_\pm(0) = 0$, Eq. (20) may be solved as $\alpha_\pm(t) = \frac{1}{\Omega_\pm}\int_0^t dt' f_\pm(t')\sin[\Omega_\pm(t - t')]$ [see Eq. (38)]. Thus the phase (48) can be also expressed by double integrals of the form

$$\phi(t_f) = \sum_{\mu=\pm}\int_0^{t_f} dt' \int_0^{t'} dt'' f_\mu(t') f_\mu(t'')\frac{\sin[\Omega_\mu(t' - t'')]}{2\hbar\Omega_\mu}$$

$$= \sum_{\mu=\pm}\int_0^{t_f}\int_0^{t_f} dt'dt'' f_\mu(t') f_\mu(t'')\frac{\sin(\Omega_\mu|t' - t''|)}{4\hbar\Omega_\mu} \tag{B1}$$

(see also [8,9,11]).

APPENDIX C: WORST CASE FIDELITY

To simplify notation, let us denote the internal state configurations by a generic index $s = \uparrow\uparrow, \uparrow\downarrow, \downarrow\uparrow, \downarrow\downarrow$. Assume an initial state $|\psi_m\rangle(\sum_s c_s|s\rangle)$, where $\sum|c_s|^2 = 1$ and the m here stands for "motional." The ideal output state, up to a global phase factor, is

$$|\psi_{id}\rangle = \left(\sum_s c_s e^{i\phi(s)}|s\rangle\right)|\psi_m\rangle, \tag{C1}$$

where

$$\phi(\uparrow\downarrow) + \phi(\downarrow\uparrow) - \phi(\uparrow\uparrow) - \phi(\downarrow\downarrow) = \pm\pi. \tag{C2}$$

The actual output state is generally entangled,

$$|\psi_{ac}\rangle = \sum_s c_s e^{i\phi'(s)}|s\rangle|\psi_{ms}\rangle, \tag{C3}$$

with a different motional state $|\psi_{ms}\rangle$ for each spin configuration, and actual phases $\phi'(s)$. First we can compute the total overlap:

$$\langle\psi_{id}|\psi_{ac}\rangle = \sum_s |c_s|^2 e^{i[\phi'(s)-\phi(s)]}\langle\psi_m|\psi_{ms}\rangle. \tag{C4}$$

Moreover, writing each motional overlap in the form $\langle\psi_m|\psi_{ms}\rangle = |\langle\psi_m|\psi_{ms}\rangle|e^{i\phi_{ms}} = \epsilon_s e^{i\phi_{ms}}$, we have

$$\langle\psi_{id}|\psi_{ac}\rangle = \sum_s |c_s|^2 \epsilon_s e^{i\delta_s} = \text{Re} + i\text{Im}, \tag{C5}$$

where $\delta_s \equiv \phi'(s) - \phi(s) + \phi_{ms}$, and

$$\mathrm{Re} = \sum_s |c_s|^2 \epsilon_s \cos \delta_s, \quad \mathrm{Im} = \sum_s |c_s|^2 \epsilon_s \sin \delta_s. \quad \text{(C6)}$$

The fidelity is

$$\mathcal{F} = |\mathrm{Re} + i\mathrm{Im}|^2 = \mathrm{Re}^2 + \mathrm{Im}^2 \geqslant \mathrm{Re}^2$$

$$= \left(\sum_s |c_s|^2 \epsilon_s \cos \delta_s \right)^2. \quad \text{(C7)}$$

Assuming a "good gate," such that $|\delta_s| \ll 1$ for all s, then the fidelity is bounded from below by the worst possible case:

$$\mathcal{F} \geqslant \mathrm{Min}[(\epsilon_s \cos \delta_s)^2]. \quad \text{(C8)}$$

$$\psi(x_1, x_2) = \left(\frac{m\sqrt{3}\omega^2}{\pi^2 \hbar^2} \right)^{1/4} e^{-\frac{m\omega}{4\hbar}[(1+\sqrt{3})(x_1+\frac{x_0}{2})^2 + (1+\sqrt{3})(x_2-\frac{x_0}{2})^2 + 2(1-\sqrt{3})(x_1+\frac{x_0}{2})(x_2-\frac{x_0}{2})]}. \quad \text{(D2)}$$

The expectation values of x_1 and x_1^2 are calculated as

$$\langle x_1 \rangle = \int_{-\infty}^{\infty} \int_{-\infty}^{\infty} dx_1 dx_2 \, x_1 \psi^2(x_1, x_2) = -\frac{x_0}{2},$$

$$\langle x_1^2 \rangle = \int_{-\infty}^{\infty} \int_{-\infty}^{\infty} dx_1 dx_2 \, x_1^2 \psi^2(x_1, x_2) = \frac{x_0^2}{4} + \frac{(3+\sqrt{3})\hbar}{12m\omega},$$

$$\text{(D3)}$$

so that the wave packet width for ion 1 is

$$\Delta x_1 = \sqrt{\langle x_1^2 \rangle - \langle x_1 \rangle^2} = \frac{1}{2}\sqrt{1 + \frac{1}{\sqrt{3}}} \sqrt{\frac{\hbar}{m\omega}}. \quad \text{(D4)}$$

APPENDIX E: ALTERNATIVE INVERSION PROTOCOLS

In the inversion protocol used in Sec. VI for different masses, we have set $\alpha_-(\uparrow\downarrow; t) = 0$ so this mode does not

APPENDIX D: SPREAD OF THE POSITION OF ONE ION IN THE GROUND STATE OF THE TWO IONS

An approximate analytical wave function for the ground state of the two ions subjected to the Hamiltonian (5) is given by multiplying the ground states of the two normal modes [see Eq. (24)]:

$$\psi_{NM} = \left(\frac{\Omega_+ \Omega_-}{\pi^2 \hbar^2} \right)^{1/4} e^{-\frac{1}{2\hbar}(\Omega_+ x_+^2 + \Omega_- x_-^2)}. \quad \text{(D1)}$$

In laboratory coordinates, and for the specific case of equal-mass ions, the normalized ground state is

produce any excitation or any phase. It is also possible to have the other mode at rest, $\alpha_+(\uparrow\downarrow; t) = 0$, by plugging in

$$\alpha_+(\uparrow\downarrow) = 0,$$

$$\alpha_-(\uparrow\downarrow) = b_0 + \sum_{n=1}^{4} b_n \cos\left[\frac{(2n-1)\pi t}{t_f} \right]. \quad \text{(E1)}$$

When choosing the alternative *Ansatz* in Eq. (E1), the critical times (72) are exactly the same. Alternatively, we may cancel one of the normal modes in the parallel configuration substituting the inversion scheme in Eq. (66) by

$$\alpha_\pm(\uparrow\uparrow) \dashrightarrow f_\pm(\uparrow\uparrow) \dashrightarrow F_a, F_b \dashrightarrow f_\pm(\uparrow\downarrow) \dashrightarrow \alpha_\pm(\uparrow\downarrow). \quad \text{(E2)}$$

This type of freedom may be useful to further minimize the forces.

[1] A. Sørensen, and K. Mølmer, Phys. Rev. Lett. **82**, 1971 (1999).

[2] E. Solano, R. L. de Matos Filho, and N. Zagury, Phys. Rev. A **59**, R2539 (1999).

[3] G. J. Milburn, S. Schneider, and D. F. V. James, Fortschr. Phys. **48**, 801 (2000).

[4] A. Sørensen and K. Mølmer, Phys. Rev. A **62**, 022311 (2000).

[5] C. A. Sackett *et al.*, Nature (London) **404**, 256 (2000).

[6] D. Leibfried, B. DeMarco, V. Meyer, D. Lucas, M. Barrett, J. Britton, W. M. Itano, B. Jelenković, C. Langer, T. Rosenband, and D. J. Wineland, Nature (London) **422**, 412 (2003).

[7] S.-L. Zhu and Z. D. Wang, Phys. Rev. Lett. **91**, 187902 (2003).

[8] J. J. García-Ripoll, P. Zoller, and J. I. Cirac, Phys. Rev. A **71**, 062309 (2005).

[9] P. Staanum, M. Drewsen, and K. Mølmer, Phys. Rev. A **70**, 052327 (2004).

[10] A. M. Steane, G. Imreh, J. P. Home, and D. Leibfried, New J. Phys. **16**, 053049 (2014).

[11] L. S. Simeonov, P. A. Ivanov, and N. V. Vitanov, Phys. Rev. A **89**, 012304 (2014).

[12] C. D. B. Bentley, A. R. R. Carvalho, D. Kielpinski, and J. J. Hope, New J. Phys. **15**, 043006 (2013).

[13] R. L. Taylor, C. D. B. Bentley, J. S. Pedernales, L. Lamata, E. Solano, A. R. R. Carvalho, and J. J. Hope, arXiv:1601.00359.

[14] L.-M. Duan, Phys. Rev. Lett. **93**, 100502 (2004).

[15] H. R. Lewis and W. B. Riesenfeld, J. Math. Phys. **10**, 1458 (1969).

[16] P. J. Lee, K.-A. Brickman, L. Deslauriers, P. C. Haljan, L.-M. Duan, and C. Monroe, J. Opt. B: Quantum Semiclass. Opt. **7**, S371 (2005).

[17] T. R. Tan, J. P. Gaebler, Y. Lin, Y. Wan, R. Bowler, D. Leibfried, and D. J. Wineland, Nature (London) **528**, 380 (2015).

[18] M. Sasura and A. M. Steane, Phys. Rev. A **67**, 062318 (2003).

[19] X. Chen, A. Ruschhaupt, S. Schmidt, A. del Campo, D. Guéry-Odelin, and J. G. Muga, Phys. Rev. Lett. **104**, 063002 (2010).

[20] E. Torrontegui, S. Ibáñez, S. Martínez-Garaot, M. Modugno, A. del Campo, D. Guéry-Odelin, A. Ruschhaupt, X. Chen, and J. G. Muga, Adv. At. Mol. Opt. Phys. **62**, 117 (2013).

[21] E. Torrontegui, S. Ibáñez, X. Chen, A. Ruschhaupt, D. Guéry-Odelin, and J. G. Muga, Phys. Rev. A **83**, 013415 (2011).

[22] M. Palmero, R. Bowler, J. P. Gaebler, D. Leibfried, and J. G. Muga, Phys. Rev. A **90**, 053408 (2014).

[23] R. Kosloff, J. Phys. Chem. **92**, 2087 (1988).

[24] R. Kosloff and H. Tal-Ezer, Chem. Phys. Lett. **127**, 223 (1986).

[25] A. Ruschhaupt, X. Chen, D. Alonso, and J. G. Muga, New J. Phys. **14**, 093040 (2012).

[26] X.-J. Lu, X. Chen, A. Ruschhaupt, D. Alonso, S. Guérin, and J. G. Muga, Phys. Rev. A **88**, 033406 (2013).

[27] X.-J. Lu, J. G. Muga, X. Chen, U. G. Poschinger, F. Schmidt-Kaler, and A. Ruschhaupt, Phys. Rev. A **89**, 063414 (2014).

[28] D. Daems, A. Ruschhaupt, D. Sugny, and S. Guérin, Phys. Rev. Lett. **111**, 050404 (2013).